CHAPTER 8

THE MONTE CARLO METHOD FOR SURFACE EXCHANGE

8.1 INTRODUCTION

Very few exact, closed-form solutions to thermal radiation problems exist, even in the absence of a participating medium. Under most circumstances the solution has to be found by numerical means. For most engineers, who are used to dealing with partial differential equations, this implies use of *finite difference* and *finite element* techniques. These methods are, of course, applicable to thermal radiation problems whenever a solution method is chosen that transforms the governing equations into sets of partial differential equations. For surface exchange, however, radiative transfer is governed by integral equations, which may be solved numerically by employing *numerical quadrature* for the evaluation of integrals, or more approximately using the "net radiation method" of the previous three chapters. With these techniques the solutions to relatively simple problems are readily found. However, if the geometry is involved, and/or if radiative properties vary with direction, then a solution by conventional numerical techniques may quickly become extremely involved if not impossible.

Many mathematical problems may also be solved by statistical methods, through sampling techniques, to any degree of accuracy. For example, consider predicting the outcome of the next presidential elections. Establishing a mathematical model that would predict voter turnout and voting behavior is, of course, impossible, let alone finding the analytical solution to such a model. However, if an appropriate sampling technique is chosen, the outcome can be predicted by conducting a poll. The accuracy of its prediction depends primarily on the sample size, i.e., how many people have been polled. Solving mathematical problems statistically always involves the use of random numbers, which may be picked, e.g., by placing a ball into a spinning roulette wheel. For this reason these sampling methods are called *Monte Carlo methods* (named after the principality of Monte Carlo in the south of France, famous for its casino). There is no single scheme to which the name *Monte Carlo* applies. Rather, any method of solving a mathematical problem with an appropriate statistical sampling technique is commonly referred to as a Monte Carlo method.

Problems in thermal radiation are particularly well suited to solution by a Monte Carlo technique, since energy travels in discrete parcels (photons) over (usually) relatively long distances along a (usually) straight path before interaction with matter. Thus, solving a thermal radiation problem by Monte Carlo implies tracing the history of a statistically meaningful random sample of photons from their points of emission to their points of absorption. The advantage of the

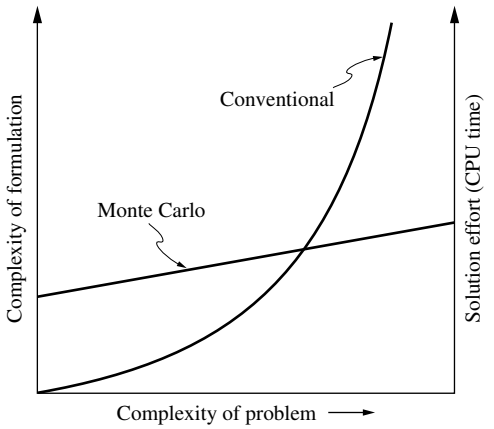

FIGURE 8-1
Comparison of Monte Carlo and conventional solution techniques.

Monte Carlo method is that even the most complicated problem may be solved with relative ease, as schematically indicated in Fig. 8-1. For a trivial problem, setting up the appropriate photon sampling technique alone may require more effort than finding the analytical solution. As the complexity of the problem increases, however, the complexity of formulation and the solution effort increase much more rapidly for conventional techniques. For problems beyond a certain complexity, the Monte Carlo solution will be preferable. Unfortunately, there is no way to determine a priori precisely where this crossover point in complexity lies. The disadvantage of Monte Carlo methods is that, as statistical methods, they are subject to statistical error (very similar to the unavoidable error associated with experimental measurements).

The name and the systematic development of Monte Carlo methods dates from about 1944 [1], although some crude mathematical sampling techniques were used off and on during previous centuries. Their first use as a research tool stems from the attempt to model neutron diffusion in fission material, for the development of the atomic bomb during World War II. The method was first applied to thermal radiation problems in the early 1960s by Fleck [2, 3] and Howell and Perlmutter [4–6].

For a thorough understanding of Monte Carlo methods, a good background in statistical methods is necessary, which goes beyond the scope of this book. In this chapter the method as applied to thermal radiation is outlined, and statistical considerations are presented in an intuitive way rather than in a rigorous mathematical fashion. For a more detailed description, the reader may want to consult the books by Hammersley and Handscomb [1], Cashwell and Everett [7], and Schreider [8], or the monographs by Kahn [9], Brown [10], Halton [11], and Hajji-Sheikh [12]. A first monograph dealing specifically with Monte Carlo methods as applied to thermal radiation has been given by Howell [13]. Another more recent one by Walters and Buckius [14] emphasizes the treatment of scattering. An exhaustive review of the literature up until 1997, that uses some form of radiative Monte Carlo analysis, has been given also by Howell [15]. Since then a large number of researchers have applied Monte Carlo simulations to a vast array of problems, ranging from nanoscale radiation properties to large-scale tomography, surface radiation, participating media, transient radiation, combined modes heat transfer, etc., too numerous to review in this book.

Probability Distributions

When a political poll is conducted, people are not selected at random from a telephone directory. Rather, people are randomly selected from different groups according to *probability distributions*, to ensure that representative numbers of barbers, housewives, doctors, smokers, gun owners, bald people, heat transfer engineers, etc. are included in the poll. Similarly, in order to follow the history of radiative energy bundles in a statistically meaningful way, the points, directions

and wavelengths of emission, reflective behavior, etc. must be chosen according to probability distributions.

As an example, consider the total radiative heat flux being emitted from a surface, i.e., the total emissive power,

$$E = \int_0^\infty E_\lambda \, d\lambda = \int_0^\infty \epsilon_\lambda E_{b\lambda} \, d\lambda. \tag{8.1}$$

Between the wavelengths of λ and $\lambda + d\lambda$ the emitted heat flux is $E_\lambda \, d\lambda = \epsilon_\lambda E_{b\lambda} \, d\lambda$, and the fraction of energy emitted over this wavelength range is

$$P(\lambda) \, d\lambda = \frac{E_\lambda \, d\lambda}{\int_0^\infty E_\lambda \, d\lambda} = \frac{E_\lambda}{E} \, d\lambda. \tag{8.2}$$

We may think of all the photons leaving the surface as belonging to a set of N energy bundles of equal energy (each consisting of many photons of a single wavelength). Then each bundle carries the amount of energy (E/N) with it, and the probability that any particular bundle has a wavelength between λ and $\lambda + d\lambda$ is given by the *probability density function* $P(\lambda)$. The fraction of energy emitted over all wavelengths between 0 and λ is then

$$R(\lambda) = \int_0^\lambda P(\lambda) \, d\lambda = \frac{\int_0^\lambda E_\lambda \, d\lambda}{\int_0^\infty E_\lambda \, d\lambda}. \tag{8.3}$$

It is immediately obvious that $R(\lambda)$ is also the probability that any given energy bundle has a wavelength between 0 and λ, and it is known as the *cumulative distribution function.* The probability that a bundle has a wavelength between 0 and ∞ is, of course, $R(\lambda \to \infty) = 1$, a certainty. Equation (8.3) implies that if we want to simulate emission from a surface with N energy bundles of equal energy, then the fraction $R(\lambda)$ of these bundles must have wavelengths smaller than λ.

Now consider a pool of random numbers equally distributed between the values 0 and 1. Since they are equally distributed, this implies that a fraction R of these random numbers have values less than R itself. Let us now pick a single random number, say R_0. Inverting equation (8.3), we find $\lambda(R_0)$, i.e., the wavelength corresponding to a cumulative distribution function of value R_0, and we assign this wavelength to one energy bundle. If we repeat this process many times, then the fraction R_0 of all energy bundles will have wavelengths below $\lambda(R_0)$, since the fraction R_0 of all our random numbers will be below this value. Thus, in order to model correctly the spectral variation of surface emission, using N bundles of equal energy, their wavelengths may be determined by picking N random numbers between 0 and 1, and inverting equation (8.3).

Random Numbers

If we throw a ball onto a spinning roulette wheel, the ball will eventually settle on any one of the wheel's numbers (between 0 and 36). If we let the roulette wheel decide on another number again and again, we will obtain a *set of random numbers* between 0 and 36 (or between 0 and 1, if we divide each number by 36). Unless the croupier throws in the ball and spins the wheel in a regular (nonrandom) fashion,[1] any number may be chosen each time with equal probability, regardless of what numbers have been picked previously. However, if sufficiently many numbers are picked, we may expect that roughly half (i.e., 18/37) of all the picked numbers will be between 0 and 17, for example.

[1]This is, of course, the reason casinos tend to employ a number of croupiers, each of whom works only for a very short period each day.

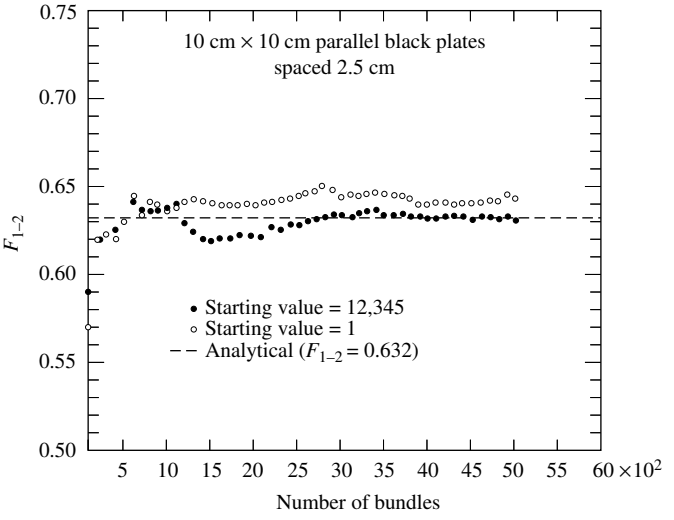

FIGURE 8-2
Convergence of Monte Carlo method for different sets of random numbers.

During the course of a Monte Carlo simulation, generally somewhere between 10^5 and 10^7 random numbers need to be drawn, and they need to be drawn very rapidly. Obviously, spinning a roulette wheel would be impractical. One solution to this problem is to store an (externally determined) set of random numbers. However, such a table would require a prohibitive amount of computer storage, unless it were a relatively small table, that would be used repeatedly (thus destroying the true randomness of the set). The only practical answer is to generate the random numbers within the computer itself. This appears to be a contradiction, since a digital computer is the incarnation of logic (nonrandomness). Substantial research has been carried out on how to generate sets of sufficiently random numbers using what are called *pseudorandom number generators.* A number of such generators exist that, after making the choice of a starting point, generate a new pseudorandom number from the previous one. The randomness of such a set of numbers depends on the quality of the generator as well as the choice of the starting point and should be tested by different "randomness tests." For a more detailed discussion of pseudorandom number generators, the reader is referred to Hammersley and Handscomb [1], Schreider [8], or Taussky and Todd [16].

Accuracy Considerations

Since Monte Carlo methods are statistical methods, the results, when plotted against number of samples, will generally fluctuate randomly around the correct answer. If a set of truly random numbers is used for the sampling, then these fluctuations will decrease as the number of samples increases. Let the answer obtained from the Monte Carlo method after tracing N energy bundles be $S(N)$, and the exact solution obtained after sampling infinitely many energy bundles $S(\infty)$. For some simple problems it is possible to calculate directly the probability that the obtained answer, $S(N)$, differs by less than a certain amount from the correct answer, $S(\infty)$.

Even if it were possible to directly calculate the confidence level for more complicated situations, this would not take into account the pseudorandomness of the computer-generated random number set. That this effect can be rather substantial is seen from Fig. 8-2, which depicts the Monte Carlo evaluation of the view factor between two parallel black plates [17]. Both sets of data use the same computer code and the same random number generator (on a UNIVAC 1110). If a starting value of 1 is used, the results are still fairly inaccurate after 5000 bundles; if a starting value of 12,345 is used (this number gave the fastest-converging results of the ones tested for the random number generator used here), good convergence is achieved after only 4000 bundles. Obviously, careful investigation of the random number generator can increase

convergence and accuracy and thus decrease computer time considerably. Randomness tests performed on sets of generated numbers showed that a starting value of 12,345 performs well in all tests and indeed results in a "better" set of random numbers than the starting value of 1 for the random number generator employed by Modest and Poon [17].

For radiative heat transfer calculations the most straightforward way of estimating the error associated with the sampling result $S(N)$ is to break up the result into a number of I subsamples $S(N_i)$, such that

$$N = N_1 + N_2 + \ldots + N_I = \sum_{i=1}^{I} N_i, \tag{8.4}$$

$$S(N) = \frac{1}{N}\left(N_1 S(N_1) + \ldots + N_I S(N_I)\right) = \frac{1}{N}\sum_{i=1}^{I} N_i S(N_i). \tag{8.5}$$

Normally, each subsample would include identical amounts of bundles, leading to

$$N_i = N/I; \qquad i = 1, 2, \ldots, I, \tag{8.6}$$

$$S(N) = \frac{1}{I}\sum_{i=1}^{I} S(N_i). \tag{8.7}$$

The I subsamples may then be treated as if they were independent experimental measurements of the same quantity. We may then calculate the *variance* or *adjusted mean square deviation of the mean*

$$\sigma_m^2 = \frac{1}{I(I-1)}\sum_{i=1}^{I}\left[S(N_i) - S(N)\right]^2. \tag{8.8}$$

The *central limit theorem* states that the mean $S(N)$ of I measurements $S(N_i)$ follows a Gaussian distribution, whatever the distribution of the individual measurements. This implies that we can say with 68.3% confidence that the correct answer $S(\infty)$ lies within the limits of $S(N) \pm \sigma_m$, with 95.5% confidence within $S(N) \pm 2\sigma_m$, or with 99% confidence within $S(N) \pm 2.58\sigma_m$. Details on statistical analysis of errors may be found in any standard book on experimentation, for example, the one by Barford [18].

8.2 NUMERICAL QUADRATURE BY MONTE CARLO

Before discussing how statistical methods can be used to solve complicated radiative transfer problems, we will quickly demonstrate that the Monte Carlo method can also be employed to evaluate integrals numerically (known as numerical quadrature). Consider the integral $\int_a^b f(x)\,dx$. The most primitive form of numerical quadrature is the *trapezoidal rule*, in which $f(x)$ is assumed constant over a small interval Δx, i.e. [19, 20],

$$\int_a^b f(x)\,dx \simeq \sum_{i=1}^{N} f\left[x_i = (i - \tfrac{1}{2})\Delta x\right]\Delta x; \quad \Delta x = \frac{b-a}{N}. \tag{8.9}$$

For large enough values of N equation (8.9) converges to the correct result. Note that the values of x_i are equally distributed across the interval between a and b. If we were to draw N random locations equally distributed between a and b, we would achieve the same result in a statistical sense. Therefore, we can evaluate any integral via the Monte Carlo method as

$$\int_a^b f(x)\,dx \simeq \sum_{i=1}^{N} f\left[x_i = a + (b-a)R_i\right]\Delta x; \; \Delta x = \frac{b-a}{N}, \tag{8.10}$$

where R_i is a set of random numbers equally distributed between 0 and 1. Equation (8.10) is an efficient means of integration if the integrand $f(x)$ is poorly behaved as, e.g., in the evaluation of k-distributions in Chapter 11 (integration over spectral variations of the absorption coefficient of molecular gases). However, if $f(x)$ varies by orders of magnitude (but in a predictable manner) across $a \le x \le b$, picking equally distributed x_i results in putting equal emphasis on important as well as unimportant regions. The stochastic integration can be made more efficient by determining the x_i from a probability density function (PDF) $p(x)$. We may write

$$\int_a^b f(x)\,dx = \int_a^b \frac{f(x)}{p(x)} p(x)\,dx = \int_0^1 \frac{f(x(\xi))}{p(x(\xi))}\,d\xi \tag{8.11}$$

where

$$\xi(x) = \int_a^x p(x)\,dx, \quad \int_a^b p(x)\,dx \equiv 1. \tag{8.12}$$

The PDF is chosen in such a way that f/p remains relatively constant across $a \le x \le b$, assuring that each stochastic sample makes roughly the same contribution to the result. The integral may then be evaluated as

$$\int_a^b f(x)\,dx \simeq \frac{b-a}{N} \sum_{i=1}^{N} \frac{f(x_i)}{p(x_i)}, \quad x_i = \xi^{-1}(R_i). \tag{8.13}$$

Equations (8.10) and (8.13) are also useful if integration is an integral part of a Monte Carlo simulation, such as the Backward Monte Carlo scheme described in Chapter 21. Finally, extension to two- and higher-dimensional integrals is obvious and trivial.

8.3 HEAT TRANSFER RELATIONS FOR RADIATIVE EXCHANGE BETWEEN SURFACES

In the absence of a participating medium and assuming a refractive index of unity, the radiative heat flux leaving or going into a certain surface, using the Monte Carlo technique, is governed by the following basic equation:

$$q(\mathbf{r}) = \epsilon(\mathbf{r})\sigma T^4(\mathbf{r}) - \int_A \epsilon(\mathbf{r}')\,\sigma T^4(\mathbf{r}') \frac{d\mathscr{F}_{dA'\to dA}}{dA}\,dA', \tag{8.14}$$

where

$q(\mathbf{r})$	=	local surface heat flux at location $\mathbf{r}$,
$T(\mathbf{r})$	=	surface temperature at location $\mathbf{r}$,
$\epsilon(\mathbf{r})$	=	total hemispherical emittance of the surface at $\mathbf{r}$,
A	=	surface area of the enclosure, and
$d\mathscr{F}_{dA'\to dA}$	=	generalized radiation exchange factor between surface elements dA' and dA.

In equation (8.14) the first term on the right-hand side describes the emission from the surface, and the integrand of the second term is the fraction of energy, originally emitted from the surface at $\mathbf{r}'$, which eventually gets absorbed at location $\mathbf{r}$. Therefore, the definition for the generalized exchange factor must be:

$$d\mathscr{F}_{dA'\to dA} \equiv \text{fraction of the total energy emitted by } dA' \text{ that is absorbed by } dA, \text{ either directly or after any number and type of reflections.} \tag{8.15}$$

This definition appears to be the most compatible one for solution by ray-tracing techniques and is therefore usually employed for calculations by the Monte Carlo method. Figure 8-3 shows a schematic of an arbitrary enclosure with energy bundles emitted at dA' and absorbed at dA.

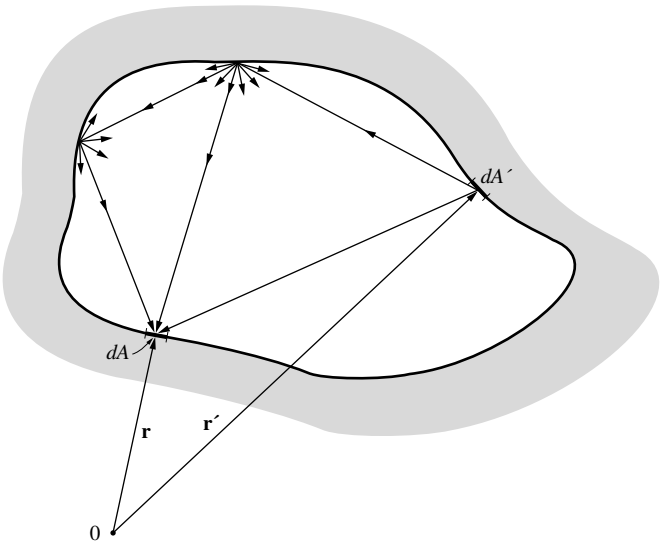

FIGURE 8-3
Possible energy bundle paths in an arbitrary enclosure.

If the enclosure is not closed, i.e., has openings into space, some artificial closing surfaces must be introduced. For example, an opening directed into outer space without irradiation from the sun or Earth can be replaced by a black surface at a temperature of 0 K. If the opening is irradiated by the sun, it is replaced by a nonreflecting surface with zero emittance for all angles but the solar angle, etc.

The enclosure surface is now divided into J subsurfaces, and equation (8.14) reduces to

$$Q_i = \int_{A_i} q_i \, dA_i = \epsilon_i \sigma T_i^4 A_i - \sum_{j=1}^{J} \epsilon_j \sigma T_j^4 A_j \mathscr{F}_{j \to i} - q_{\text{ext}} A_s \mathscr{F}_{s \to i}, \quad 1 \le i \le J, \tag{8.16}$$

where

q_{ext} = external energy entering through any opening in the enclosure,
A_s = area of the opening irradiated from external sources,

and the ϵ_j and T_j are suitable average values for each subsurface, i.e.,

$$\epsilon_j \sigma T_j^4 = \frac{1}{A_j} \int_{A_j} \epsilon \sigma T^4 \, dA. \tag{8.17}$$

Although heat flow rates Q_i can be calculated directly by the Monte Carlo method, it is of advantage to instead determine the exchange factors: Although the Q_i's depend on all surface temperatures in the enclosure, the $\mathscr{F}_{i \to j}$'s either do not (gray surfaces) or depend only on the temperature of the emitting surface (nongray surfaces), provided that surface reflectances (and absorptances) are independent of temperature (as they are to a very good degree of accuracy). Since all emitted energy must go somewhere, and, by the Second Law of Thermodynamics the net exchange between two equal temperature surfaces must be zero, the summation rule and reciprocity also hold for exchange factors, i.e.,

$$\sum_{j=1}^{J} \mathscr{F}_{i \to j} = 1, \tag{8.18}$$

$$\epsilon_i A_i \mathscr{F}_{i \to j} = \epsilon_j A_j \mathscr{F}_{j \to i}, \tag{8.19}$$

(the former, of course, only for enclosures without openings).

A large statistical sample of energy bundles N_i is emitted from surface A_i, each of them carrying the amount of radiative energy

$$\Delta E_i = \epsilon_i \sigma T_i^4 A_i / N_i. \tag{8.20}$$

If N_{ij} of these bundles become absorbed by surface A_j either after direct travel or after any number of reflections, the exchange factor may be calculated from

$$\mathscr{F}_{i\to j} = \lim_{N_i\to\infty}\left(\frac{N_{ij}}{N_i}\right) \simeq \left(\frac{N_{ij}}{N_i}\right)_{N_i\gg 1}. \tag{8.21}$$

`MONT3D` is a publicly available Fortran code [21–24], given in Appendix F, that calculates general exchange factors for complicated three-dimensional geometries. Monte Carlo calculations of exchange factors, by their nature, automatically obey the summation rule, equation (8.18), but—due to the inherent statistical scatter—reciprocity, equation (8.19), is not fulfilled. Several smoothing schemes have been given in the literature that assure that both equations (8.18) and (8.19) are satisfied [25–29].

8.4 RANDOM NUMBER RELATIONS FOR SURFACE EXCHANGE

In order to calculate the exchange factor by tracing the history of a large number of energy bundles, we need to know how to pick statistically meaningful energy bundles as explained in Section 8.1: for each emitted bundle we need to determine a point of emission, a direction of emission, and a wavelength of emission. Upon impact of the bundle onto another point of the enclosure surface, we need to decide whether the bundle is reflected and, if so, into what direction.

Points of Emission

Similar to equation (8.1) we may write for the total emission from a surface A_j:

$$E_j = \int_{A_j} \epsilon\sigma T^4\, dA. \tag{8.22}$$

Since integration over an area is a double integral, we may rewrite this equation, without loss of generality, as

$$E_j = \int_{x=0}^{X}\int_{y=0}^{Y} \epsilon\sigma T^4 dy\, dx = \int_0^X E'_j\, dx, \tag{8.23}$$

where

$$E'_j(x) = \int_0^Y \epsilon\sigma T^4 dy. \tag{8.24}$$

Thus, we may apply equation (8.3) and find

$$R_x = \frac{1}{E_j}\int_0^x E'_j\, dx. \tag{8.25}$$

This relationship may be inverted to find the x-location of the emission point as a function of a random number R_x:

$$x = x(R_x). \tag{8.26}$$

Once the x-location has been determined, equation (8.3) may also be applied to equation (8.24), leading to an expression for the y-location of emission:

$$R_y = \frac{1}{E'_j(x)}\int_0^y \epsilon\sigma T^4 dy, \tag{8.27}$$

and

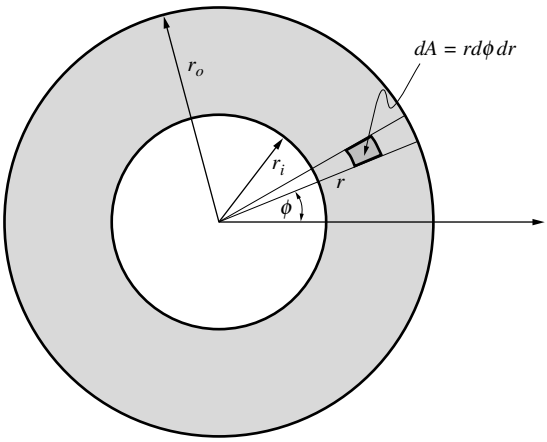

FIGURE 8-4
Geometry for Example 8.1.

$$y = y(R_y, x). \tag{8.28}$$

Note that the choice for the y-location depends not only on the random number R_y, but also on the location of x.

If the emissive power may be separated in x and y, i.e., if

$$E = \epsilon\sigma T^4 = E_x(x)E_y(y), \tag{8.29}$$

then equation (8.25) reduces to

$$R_x = \int_0^x E_x(x)\, dx \Big/ \int_0^X E_x(x)\, dx, \tag{8.30}$$

and equation (8.27) simplifies to

$$R_y = \int_0^y E_y(y)\, dy \Big/ \int_0^Y E_y(y)\, dy, \tag{8.31}$$

that is, choices for x- and y-locations become independent of one another. In the simplest case of an isothermal surface with constant emittance, these relations reduce to

$$x = R_x X, \quad y = R_y Y. \tag{8.32}$$

Example 8.1. Given a ring surface element on the bottom of a black isothermal cylinder with inner radius $r_i = 10$ cm and outer radius $r_o = 20$ cm, as indicated in Fig. 8-4, calculate the location of emission for a pair of random numbers $R_r = 0.5$ and $R_\phi = 0.25$.

Solution
We find

$$E = \int_A E_b\, dA = E_b \int_0^{2\pi} \int_{r_i}^{r_o} r\, dr\, d\phi.$$

Since this expression is separable in r and ϕ, this leads to

$$R_\phi = \int_0^\phi d\phi \Big/ \int_0^{2\pi} d\phi = \frac{\phi}{2\pi}, \quad \text{or} \quad \phi = 2\pi R_\phi,$$

and

$$R_r = \int_{r_i}^r r\, dr \Big/ \int_{r_i}^{r_o} r\, dr = \frac{r^2 - r_i^2}{r_o^2 - r_i^2},$$

or

$$r = \sqrt{r_i^2 + (r_o^2 - r_i^2)R_r}.$$

Therefore, $\phi = 2\pi \times 0.25 = \pi/2$ and $r = \sqrt{100 + (400 - 100)0.5} = 15.8\,\text{cm}$. While, as expected for a random number of 0.25, the emission point angle is 90° away from the $\phi = 0$ axis, the r-location does not fall onto the midpoint. This is because the cylindrical ring has more surface area at larger radii, resulting in larger total emission. This implies that more energy bundles must be emitted from the outer part of the ring.

Wavelengths of Emission

Once an emission location has been chosen, the wavelength of the emitted bundle needs to be determined (unless all surfaces in the enclosure are gray; in that case the wavelength of the bundle does not enter the calculations, and its determination may be omitted). The process of finding the wavelength has already been outlined in Section 8.1, leading to equation (8.3), i.e.,

$$R_\lambda = \frac{1}{\epsilon\sigma T^4}\int_0^\lambda \epsilon_\lambda E_{b\lambda}\, d\lambda, \tag{8.33}$$

and, after inversion,

$$\lambda = \lambda(R_\lambda, x, y). \tag{8.34}$$

We note that the choice of wavelength, in general, depends on the choice for the emission location (x, y), unless the surface is isothermal with constant emittance. If the surface is black or gray, equation (8.33) reduces to the simple case of

$$R_\lambda = \frac{1}{\sigma T^4}\int_0^\lambda E_{b\lambda}\, d\lambda = f(\lambda T). \tag{8.35}$$

Directions of Emission

The spectral emissive power (for a given position and wavelength) is

$$E_\lambda = \int_{2\pi} \epsilon'_\lambda I_{b\lambda}\cos\theta\, d\Omega = \frac{1}{\pi}E_{b\lambda}\int_0^{2\pi}\int_0^{\pi/2}\epsilon'_\lambda \cos\theta\sin\theta\, d\theta\, d\psi. \tag{8.36}$$

As we did for choosing the (two-dimensional) point of emission, we write

$$R_\psi = \frac{E_{b\lambda}}{\pi E_\lambda}\int_0^\psi\int_0^{\pi/2}\epsilon'_\lambda\cos\theta\sin\theta\, d\theta\, d\psi = \frac{1}{\pi}\int_0^\psi\int_0^{\pi/2}\frac{\epsilon'_\lambda}{\epsilon_\lambda}\cos\theta\sin\theta\, d\theta\, d\psi, \tag{8.37}$$

or

$$\psi = \psi(R_\psi, x, y, \lambda). \tag{8.38}$$

We note from equation (8.37) that ψ does not usually depend on emission location, unless the emittance changes across the surface. However, ψ does depend on the chosen wavelength, unless spectral and directional dependence of the emittance are separable. Once the azimuthal angle ψ is found, the polar angle θ is determined from

$$R_\theta = \int_0^\theta \epsilon'_\lambda\cos\theta\sin\theta\, d\theta \Big/ \int_0^{\pi/2}\epsilon'_\lambda\cos\theta\sin\theta\, d\theta, \tag{8.39}$$

or

$$\theta = \theta(R_\theta, x, y, \lambda, \psi). \tag{8.40}$$

Most surfaces tend to be isotropic so that the directional emittance does not depend on azimuthal angle ψ. In that case $\epsilon_\lambda = 2\int_0^{\pi/2}\epsilon'_\lambda\cos\theta\sin\theta\, d\theta$, and equation (8.37) reduces to

$$R_\psi = \frac{\psi}{2\pi}, \quad \text{or} \quad \psi = 2\pi R_\psi, \tag{8.41}$$

and the choice of polar angle becomes independent of azimuthal angle. For a diffuse emitter, equation (8.39) simplifies to

$$R_\theta = \sin^2\theta, \quad \text{or} \quad \theta = \sin^{-1}\sqrt{R_\theta}. \tag{8.42}$$

Order of Evaluation

In the foregoing we have chosen to first determine an emission location, followed by an emission wavelength and, finally, the direction of emission, as is most customary. However, the only constraint that we need to satisfy in a statistical manner is the total emitted energy from a surface, given by

$$E = \int_A \epsilon\sigma T^4\, dA = \int_A \int_0^\infty \int_{2\pi} \epsilon'_\lambda I_{b\lambda} \cos\theta\, d\Omega\, d\lambda\, dA. \tag{8.43}$$

While we have obtained the random number relationships by peeling the integrals in equation (8.43) in the order shown, integration may be carried out in arbitrary order (e.g., first evaluating emission wavelength, etc.).

Absorption and Reflection

When radiative energy impinges on a surface, the fraction α'_λ will be absorbed, which may depend on the wavelength of irradiation, the direction of the incoming rays, and, perhaps, the local temperature. Of many incoming bundles the fraction α'_λ will therefore be absorbed while the rest, $1-\alpha'_\lambda$, will be reflected. This can clearly be simulated by picking a random number, R_α, and comparing it with α'_λ: If $R_\alpha \le \alpha'_\lambda$, the bundle is absorbed, while if $R_\alpha > \alpha'_\lambda$, it is reflected.

The direction of reflection depends on the bidirectional reflection function of the material. The fraction of energy reflected into all possible directions is equal to the directional–hemispherical spectral reflectance, or

$$\begin{aligned}\rho'^{\frown}_\lambda(\lambda,\theta_i,\psi_i) &= \int_{2\pi} \rho''_\lambda(\lambda,\theta_i,\psi_i,\theta_r,\psi_r)\cos\theta_r\, d\Omega_r \\ &= \int_0^{2\pi}\int_0^{\pi/2} \rho''_\lambda(\lambda,\theta_i,\psi_i,\theta_r,\psi_r)\cos\theta_r\sin\theta_r\, d\theta_r\, d\psi_r.\end{aligned} \tag{8.44}$$

As before, the direction of reflection may then be determined from

$$R_{\psi_r} = \frac{1}{\rho'^{\frown}_\lambda}\int_0^{\psi_r}\int_0^{\pi/2} \rho''_\lambda(\lambda,\theta_i,\psi_i,\theta_r,\psi_r)\cos\theta_r\sin\theta_r\, d\theta_r\, d\psi_r, \tag{8.45}$$

and

$$R_{\theta_r} = \frac{\displaystyle\int_0^{\theta_r} \rho''_\lambda(\lambda,\theta_i,\psi_i,\theta_r,\psi_r)\cos\theta_r\sin\theta_r\, d\theta_r}{\displaystyle\int_0^{\pi/2} \rho''_\lambda(\lambda,\theta_i,\psi_i,\theta_r,\psi_r)\cos\theta_r\sin\theta_r\, d\theta_r}. \tag{8.46}$$

If the surface is a diffuse reflector, i.e., $\rho''_\lambda(\lambda,\theta_i,\psi_i,\theta_r,\psi_r) = \rho''_\lambda(\lambda) = \rho'^{\frown}_\lambda(\lambda)/\pi$, then equations (8.45) and (8.46) reduce to

$$R_{\psi_r} = \frac{\psi_r}{2\pi}, \quad \text{or} \quad \psi_r = 2\pi R_{\psi_r}, \tag{8.47}$$

and

$$R_{\theta_r} = \sin^2\theta_r, \quad \text{or} \quad \theta_r = \sin^{-1}\sqrt{R_{\theta_r}}, \tag{8.48}$$

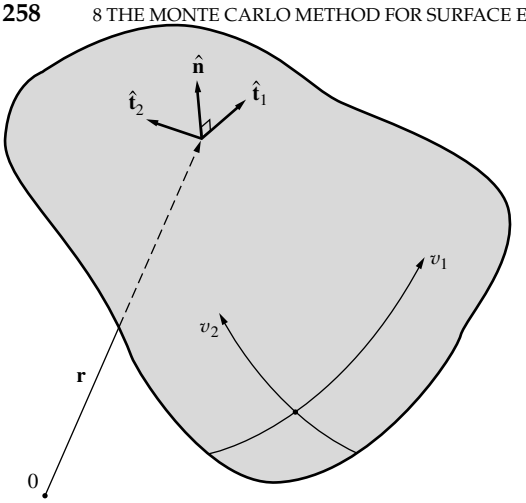

FIGURE 8-5
Surface description in terms of a position vector.

which are the same as for diffuse emission. For a purely specular reflector, the reflection direction follows from the law of optics as

$$\psi_r = \psi_i + \pi, \quad \theta_r = \theta_i, \tag{8.49}$$

that is, no random numbers are needed.[2]

8.5 SURFACE DESCRIPTION

When Monte Carlo simulations are applied to very simple configurations such as flat plates, e.g., Toor and Viskanta [30], the surface description, bundle intersection points, intersection angles, reflection angles, etc. are relatively obvious and straightforward. If more complicated surfaces are considered, such as the second-order polynomial description by Weiner and coworkers [31] or the arbitrary-order polynomial description by Modest and Poon [17] and Modest [32], a systematic way to describe surfaces is preferable. It appears most logical to describe surfaces in vectorial form, as indicated in Fig. 8-5,

$$\mathbf{r} = \sum_{i=1}^{3} x_i(v_1, v_2)\, \hat{\mathbf{e}}_i, \quad v_{1\min} \le v_1 \le v_{1\max}, \quad v_{2\min}(v_1) \le v_{2\max}(v_1), \tag{8.50}$$

that is, $\mathbf{r}$ is the vector pointing from the origin to a point on the surface, v_1 and v_2 are two surface parameters, the x_i are the (x, y, z) coordinates of the surface point, and the $\hat{\mathbf{e}}_i$ are unit vectors $(\hat{\mathbf{i}}, \hat{\mathbf{j}}, \hat{\mathbf{k}})$ into the x, y, z directions, respectively. We may define two unit tangents to the surface at any point as

$$\hat{\mathbf{t}}_1 = \frac{\partial \mathbf{r}}{\partial v_1} \Big/ \left| \frac{\partial \mathbf{r}}{\partial v_1} \right|, \quad \hat{\mathbf{t}}_2 = \frac{\partial \mathbf{r}}{\partial v_2} \Big/ \left| \frac{\partial \mathbf{r}}{\partial v_2} \right|. \tag{8.51}$$

While it is usually a good idea to choose the surface parameters v_1 and v_2 perpendicular to one another (making $\hat{\mathbf{t}}_1$ and $\hat{\mathbf{t}}_2$ perpendicular to each other), this is not necessary. In either case, one can evaluate the unit surface normal as

$$\hat{\mathbf{n}} = \frac{\hat{\mathbf{t}}_1 \times \hat{\mathbf{t}}_2}{|\hat{\mathbf{t}}_1 \times \hat{\mathbf{t}}_2|}, \tag{8.52}$$

where it has been assumed that v_1 and v_2 have been ordered such that $\hat{\mathbf{n}}$ is the *outward* surface normal.

[2]Mathematically, equation (8.49) may also be obtained from equations (8.45) and (8.46) by replacing ρ''_λ by an appropriate Dirac-delta function.

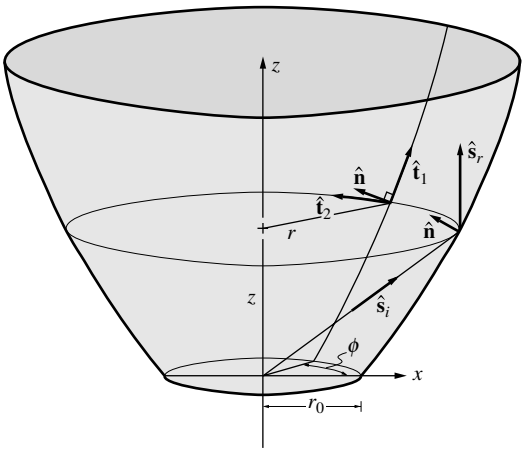

FIGURE 8-6
Rocket nozzle diffuser geometry for Example 8.2.

8.6 RAY TRACING

Points of emission may be found by establishing a relationship such as equation (8.22) for the general vectorial surface description given by equation (8.50). The infinitesimal area element on the surface may be described by

$$dA = \left|\frac{\partial \mathbf{r}}{\partial v_1} \times \frac{\partial \mathbf{r}}{\partial v_2}\right| dv_1\, dv_2 = |\hat{\mathbf{t}}_1 \times \hat{\mathbf{t}}_2| \left|\frac{\partial \mathbf{r}}{\partial v_1}\right| \left|\frac{\partial \mathbf{r}}{\partial v_2}\right| dv_1\, dv_2. \tag{8.53}$$

Thus, if we replace x by v_1 and y by v_2, emission points (v_1, v_2) are readily found from equations (8.25) and (8.27).

Example 8.2. Consider the axisymmetric rocket nozzle diffuser shown in Fig. 8-6. Assuming that the diffuser is gray and isothermal, establish the appropriate random number relationships for the determination of emission points.

Solution
The diffuser surface is described by the formula

$$z = a(r^2 - r_0^2), \quad 0 \le z \le L, \quad r_0 \le r \le r_L, \quad a = \frac{1}{2r_0},$$

where L is the length of the diffuser and r_0 and r_L are its radius at $z = 0$ and L, respectively. In vectorial form, we may write

$$\mathbf{r} = r\cos\phi\hat{\mathbf{i}} + r\sin\phi\hat{\mathbf{j}} + a(r^2 - r_0^2)\hat{\mathbf{k}},$$

where ϕ is the azimuthal angle in the x-y-plane, measured from the x-axis. This suggests the choice $v_1 = r$ and $v_2 = \phi$. The two surface tangents are now readily calculated as

$$\begin{aligned} \hat{\mathbf{t}}_1 &= \frac{\cos\phi\hat{\mathbf{i}} + \sin\phi\hat{\mathbf{j}} + 2ar\hat{\mathbf{k}}}{\sqrt{1 + 4a^2r^2}}, \\ \hat{\mathbf{t}}_2 &= -\sin\phi\hat{\mathbf{i}} + \cos\phi\hat{\mathbf{j}}. \end{aligned}$$

It is seen that $\hat{\mathbf{t}}_1 \cdot \hat{\mathbf{t}}_2 = 0$, i.e., the tangents are perpendicular to one another. The surface normal is then

$$\hat{\mathbf{n}} = \hat{\mathbf{t}}_1 \times \hat{\mathbf{t}}_2 = \frac{1}{\sqrt{1 + 4a^2r^2}} \begin{pmatrix} \hat{\mathbf{i}} & \hat{\mathbf{j}} & \hat{\mathbf{k}} \\ \cos\phi & \sin\phi & 2ar \\ -\sin\phi & \cos\phi & 0 \end{pmatrix} = \frac{-2ar(\cos\phi\hat{\mathbf{i}} + \sin\phi\hat{\mathbf{j}}) + \hat{\mathbf{k}}}{\sqrt{1 + 4a^2r^2}},$$

and, finally, an infinitesimal surface area is

$$dA = |\cos\phi\hat{\mathbf{i}} + \sin\phi\hat{\mathbf{j}} + 2ar\hat{\mathbf{k}}\| - r\sin\phi\hat{\mathbf{i}} + r\cos\phi\hat{\mathbf{j}}|\, dr\, d\phi = \sqrt{1 + 4a^2r^2}\, r\, dr\, d\phi.$$

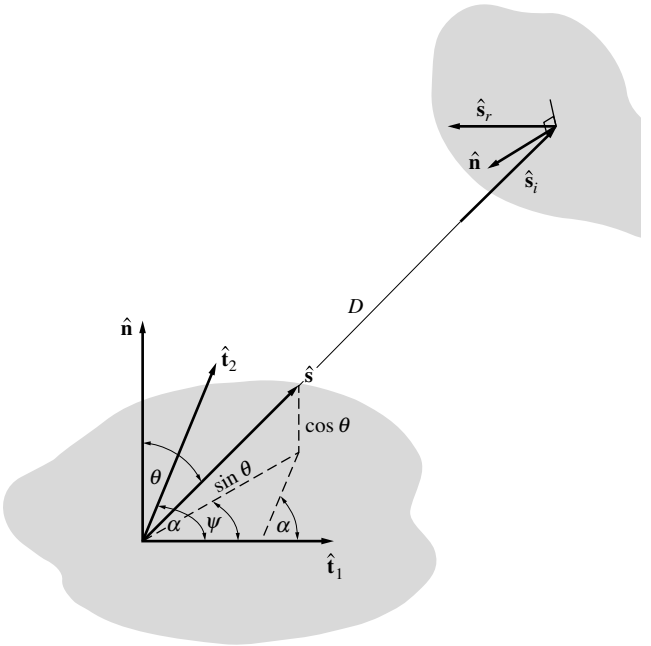

FIGURE 8-7
Vector description of emission direction and point of impact.

Since there is no dependence on azimuthal angle ϕ in either dA or the emissive power, we find immediately

$$R_\phi = \frac{\phi}{2\pi}, \quad \text{or} \quad \phi = 2\pi R_\phi,$$

and for the radial position parameter

$$R_r = \frac{\int_{r_0}^{r} \sqrt{1+4a^2r^2}\, r\, dr}{\int_{r_0}^{r_L} \sqrt{1+4a^2r^2}\, r\, dr} = \frac{(1+4a^2r^2)^{3/2}\big|_{r_0}^{r}}{(1+4a^2r^2)^{3/2}\big|_{r_0}^{r_L}} = \frac{(1+4a^2r^2)^{3/2} - (1+4a^2r_0^2)^{3/2}}{(1+4a^2r_L^2)^{3/2} - (1+4a^2r_0^2)^{3/2}}.$$

The above expression is readily solved to give an explicit expression for $r = r(R_r)$.

Once a point of emission has been found, a wavelength and a direction are calculated from equations (8.33), (8.37), and (8.39). As shown in Fig. 8-7, the direction may be specified as a *unit direction vector* with polar angle θ measured from the surface normal, and azimuthal angle ψ measured from $\hat{\mathbf{t}}_1$, leading to

$$\hat{\mathbf{s}} = \frac{\sin\theta}{\sin\alpha}\left[\sin(\alpha-\psi)\hat{\mathbf{t}}_1 + \sin\psi\hat{\mathbf{t}}_2\right] + \cos\theta\hat{\mathbf{n}}, \tag{8.54}$$

and

$$\sin\alpha = \left|\hat{\mathbf{t}}_1 \times \hat{\mathbf{t}}_2\right|, \tag{8.55}$$

where α is the angle between $\hat{\mathbf{t}}_1$ and $\hat{\mathbf{t}}_2$. If $\hat{\mathbf{t}}_1$ and $\hat{\mathbf{t}}_2$ are perpendicular ($\alpha = \pi/2$), equation (8.54) reduces to

$$\hat{\mathbf{s}} = \sin\theta\left[\cos\psi\hat{\mathbf{t}}_1 + \sin\psi\hat{\mathbf{t}}_2\right] + \cos\theta\hat{\mathbf{n}}. \tag{8.56}$$

As also indicated in Fig. 8-7, the intersection point of an energy bundle emitted at location $\mathbf{r}_e$, traveling into the direction $\hat{\mathbf{s}}$, with a surface described in vectorial form may be determined as

$$\mathbf{r}_e + D\hat{\mathbf{s}} = \mathbf{r}, \tag{8.57}$$

where $\mathbf{r}$ is the vector describing the intersection point, and D is the distance traveled by the energy bundle. Equation (8.57) may be written in terms of its x, y, z components and solved for

D by forming the dot products with unit vectors $\hat{\mathbf{i}}, \hat{\mathbf{j}}$, and $\hat{\mathbf{k}}$:

$$D = \frac{x(v_1, v_2) - x_e}{\hat{\mathbf{s}} \cdot \hat{\mathbf{i}}} = \frac{y(v_1, v_2) - y_e}{\hat{\mathbf{s}} \cdot \hat{\mathbf{j}}} = \frac{z(v_1, v_2) - z_e}{\hat{\mathbf{s}} \cdot \hat{\mathbf{k}}}. \tag{8.58}$$

Equation (8.58) is a set of three equations in the three unknowns v_1, v_2, and D: First v_1 and v_2 are calculated, and it is determined whether the intersection occurs within the confines of the surface under scrutiny. If so, and if more than one intersection is a possibility (in the presence of convex surfaces, protruding corners, etc.), then the path length D is also determined; if more than one intersection is found, the correct one is the one after the shortest positive path.

If the bundle is reflected, and if reflection is nonspecular, a reflection direction is chosen from equations (8.45) and (8.46). This direction is then expressed in vector form using equation (8.54). If the surface is a specular reflector, the direction of reflection is determined from equation (8.49), or in vector form as

$$\hat{\mathbf{s}}_r = \hat{\mathbf{s}}_i + 2|\hat{\mathbf{s}}_i \cdot \hat{\mathbf{n}}|\hat{\mathbf{n}}. \tag{8.59}$$

Once the intersection point and the direction of reflection have been determined, a new intersection may be found from equation (8.58), etc., until the bundle is absorbed.

Example 8.3. Consider again the geometry of Example 8.2. An energy bundle is emitted from the origin ($x = y = z = 0$) into the direction $\hat{\mathbf{s}} = 0.8\hat{\mathbf{i}} + 0.6\hat{\mathbf{k}}$. Determine the intersection point on the diffuser and the direction of reflection, assuming the diffuser to be a specular reflector.

Solution
With $r_e = 0$ and equations (8.54) and (8.58), we find

$$D = \frac{r\cos\phi}{0.8} = \frac{r\sin\phi}{0} = \frac{a(r^2 - r_0^2)}{0.6}.$$

Obviously, $\phi = 0$,[3] and solving the quadratic equation for r,

$$r^2 - r_0^2 = \frac{3}{4}\frac{r}{a} = \tfrac{3}{2}rr_0, \text{ or } r = 2r_0 \text{ and } z = \frac{1}{2r_0}(4r_0^2 - r_0^2) = \tfrac{3}{2}r_0.$$

At that location we form the unit vectors as given in Example 8.2,

$$\hat{\mathbf{t}}_1 = \frac{1}{\sqrt{5}}(\hat{\mathbf{i}} + 2\hat{\mathbf{k}}),\ \hat{\mathbf{t}}_2 = \hat{\mathbf{j}}, \text{ and } \hat{\mathbf{n}} = \frac{1}{\sqrt{5}}(-2\hat{\mathbf{i}} + \hat{\mathbf{k}}).$$

Therefore, the direction of reflection is determined from equation (8.59) as

$$\hat{\mathbf{s}}_r = 0.8\hat{\mathbf{i}} + 0.6\hat{\mathbf{k}} + 2\left|\frac{-2 \times 0.8 + 0.6}{\sqrt{5}}\right| \frac{-2\hat{\mathbf{i}} + \hat{\mathbf{k}}}{\sqrt{5}} = \hat{\mathbf{k}},$$

as is easily verified from Fig. 8-6.

8.7 EFFICIENCY CONSIDERATIONS

The accuracy of results for generalized radiation exchange factors or wall heat fluxes, as characterized by the standard deviation, equation (8.8), is determined by the statistical scatter of the results. The scatter may be expected to be inversely proportional to the number of bundles absorbed by a subsurface. This number of bundles, on the other hand, is directly proportional to both total number of bundles and size of subsurface. Thus, in order to achieve good spatial resolution (small element sizes), very large numbers of bundles—often several million or even billions—must be emitted and traced. Consequently, even with the availability of today's fast digital computers, it is imperative that the Monte Carlo implementation and its ray tracings be as numerically efficient as possible, if many hours of CPU time for each computer run are to be avoided. Today's trend toward massively parallel computing brings new efficiency challenges with it that—while beyond the scope of this book—have been discussed in some detail by several investigators [15].

[3] In computer calculations care must be taken here and elsewhere to avoid division by zero.

Inversion of Random Number Relations

Many of the random number relationships governing emission location, wavelength, direction, etc., cannot be inverted explicitly. For example, to determine the wavelength of emission, even for a simple black surface, for a given random number R_λ requires the solution of the transcendental equation (8.33),

$$R_\lambda = \frac{1}{\sigma T^4} \int_0^\lambda E_{b\lambda}\, d\lambda = f(\lambda T). \tag{8.60}$$

In principle, this requires guessing a λ, calculating R_λ, etc. until the correct wavelength is found; this would then be repeated for each emitted photon bundle. It would be much more efficient to invert equation (8.60) once and for all before the first energy bundle is traced as

$$\lambda T = f^{-1}(R_\lambda). \tag{8.61}$$

This is done by first calculating $R_{\lambda,j}$ corresponding to a $(\lambda T)_j$ for a sufficient number of points $j = 0, 1, \ldots, J$. These data points may then be used to obtain a polynomial description

$$\lambda T = A + BR_\lambda + CR_\lambda^2 + \cdots, \tag{8.62}$$

as proposed by Howell [13]. With the math libraries available today on most digital computers it would, however, be preferable to invert equation (8.61) using a (cubic) spline.

Even more efficient is the method employed by Modest and Poon [17] and Modest [32], who used a cubic spline to determine values of $(\lambda T)_j$ for $(J + 1)$ equally spaced random numbers

$$(\lambda T)_j = f^{-1}\left(R_\lambda = \frac{j}{J}\right), \quad j = 0, 1, 2, \ldots, J. \tag{8.63}$$

If, for example, a random number $R_\lambda = 0.6789$ is picked, it is immediately known that (λT) lies between $(\lambda T)_m$ and $(\lambda T)_{m+1}$, where m is the largest integer less than $J \times R_\lambda$ (= 67 if $J = 100$). The actual value for (λT) may then be found by (linear) interpolation.

The quantity to be determined may depend on more than a single random number. For example, to fix an emission wavelength on a surface with nonseparable emissive power (say a surface in the x-y-plane with locally varying, nongray emittance) requires the determination of

$$x = x(R_x), \quad y = y(R_y, x), \quad \lambda = \lambda(R_\lambda, x, y). \tag{8.64}$$

That is, first the x-location is chosen, requiring the interpolation between and storage of J data points $x_j(R_j)$; next the y-location is determined, requiring a double interpolation and storage of a $J \times K$ array for $y_{jk}(R_k, x_j)$; and finally λ is found from a triple interpolation from a $J \times K \times L$ array for $\lambda_{jkl}(R_l, x_j, y_k)$. This may lead to excessive computer storage requirements if J, K, L are chosen too large: If $J = K = L = 100$, an array with one million numbers needs to be stored for the determination of emission wavelengths alone! The problem may be alleviated by choosing a better interpolation scheme together with smaller values for J, K, L (for example, a choice of $J = K = L = 40$ reduces storage requirements to 64,000 numbers).

Energy Partitioning

In the general Monte Carlo method, a ray of fixed energy content is traced until it is absorbed. In the absence of a participating medium, the decision whether the bundle is absorbed or reflected is made after every impact on a surface. Thus, on the average it will take $1/\alpha$ tracings until the bundle is absorbed. Therefore, it takes $1/\alpha$ tracings to add one statistical sample to the calculation of one of the $\mathscr{F}_{i\to j}$'s. If the configuration has openings, a number of bundles may be reflected a few times before they escape into space without adding a statistical sample to any of the $\mathscr{F}_{i\to j}$'s. Thus, the ordinary Monte Carlo method becomes extremely inefficient for open configurations

and/or highly reflective surfaces. The former problem may be alleviated by partitioning the energy of emitted bundles. This was first applied by Sparrow and coworkers [33, 34], who, before determining a direction of emission, split the energy of the bundle into two parts: the part leaving the enclosure through the opening (equal to the view factor from the emission point to the opening) and the rest (which will strike a surface). A direction is then determined, limited to those that make the bundle hit an enclosure surface. The procedure is repeated after every reflection. This method guarantees that each bundle will contribute to the statistical sample for exchange factor evaluation. A somewhat more general and more easily implemented energy partitioning scheme was applied by Modest and Poon [17, 32]: Rather than drawing a random number R_α to decide whether a bundle is (fully) absorbed or not, they partition the energy of a bundle at each reflection into the fraction α, which is absorbed, and the fraction $\rho = 1 - \alpha$, which is reflected. The bundle is then traced until it either leaves the enclosure or until its energy is depleted (below a certain fraction of original energy content). This method adds to the statistical sample of a $\mathscr{F}_{i\to j}$ after *every* tracing and thus leads to vastly faster convergence for highly reflective surfaces.

Data Smoothing

Virtually all Monte Carlo implementation to date have been of 0th order, i.e., all properties within a given cell are considered constant throughout the cell, without connectivity to surrounding cells. This makes the estimation of local gradients difficult, if not impossible. Several smoothing schemes have been proposed for the exchange factors of equation (8.21), the simpler ones without restrictions on the size of corrections [26, 27], and others that find the smallest corrections that make the exchange factors satisfy, both, the summation and reciprocity relationships [28, 29].

Other Efficiency Improvements

Other improvements are often connected to the particular geometry under scrutiny. For instance, large amounts of computer time may be wasted because it is not immediately known, which of the many subsurfaces the traveling bundle will hit. In general, an intersection between every surface and the bundle must be calculated. Only then can it be determined whether this intersection is legitimate, i.e., whether it occurs within the bounds of the surface. Often the overall enclosure can be broken up into a (relatively small) number of basic surfaces (dictated by geometry), which in turn are broken up into a number of smaller, isothermal subsurfaces. Furthermore, a bundle emitted or reflected from some subsurface may not be able to hit some basic surface by any path. In other cases, if a possible point of impact on some surface has been determined, it may not be necessary to check the remaining surfaces, etc. There are no fixed rules for the computational structure of a Monte Carlo code. In these applications the proverbial "dash of ingenuity" can go a long way in making a computation efficient.

References

1. Hammersley, J. M., and D. C. Handscomb: *Monte Carlo Methods*, John Wiley & Sons, New York, 1964.
2. Fleck, J. A.: "The calculation of nonlinear radiation transport by a Monte Carlo method," Technical Report UCRL-7838, Lawrence Radiation Laboratory, 1961.
3. Fleck, J. A.: "The calculation of nonlinear radiation transport by a Monte Carlo method: Statistical physics," *Methods in Computational Physics*, vol. 1, pp. 43–65, 1961.
4. Howell, J. R., and M. Perlmutter: "Monte Carlo solution of thermal transfer through radiant media between gray walls," *ASME Journal of Heat Transfer*, vol. 86, no. 1, pp. 116–122, 1964.
5. Howell, J. R., and M. Perlmutter: "Monte Carlo solution of thermal transfer in a nongrey nonisothermal gas with temperature dependent properties," *AIChE Journal*, vol. 10, no. 4, pp. 562–567, 1964.
6. Perlmutter, M., and J. R. Howell: "Radiant transfer through a gray gas between concentric cylinders using Monte Carlo," *ASME Journal of Heat Transfer*, vol. 86, no. 2, pp. 169–179, 1964.
7. Cashwell, E. D., and C. J. Everett: *A Practical Manual on the Monte Carlo Method for Random Walk Problems*, Pergamon Press, New York, 1959.

8. Schreider, Y. A.: *Method of Statistical Testing – Monte Carlo Method*, Elsevier, New York, 1964.
9. Kahn, H.: "Applications of Monte Carlo," *Report for Rand Corp.*, vol. Rept. No. RM-1237-AEC (AEC No. AECU-3259), 1956.
10. Brown, G. W.: "Monte Carlo methods," in *Modern Mathematics for the Engineer*, McGraw-Hill, New York, pp. 279–307, 1956.
11. Halton, J. H.: "A retrospective and prospective survey of the Monte Carlo method," *SIAM Rev.*, vol. 12, no. 1, pp. 1–63, 1970.
12. Haji-Sheikh, A.: "Monte Carlo methods," in *Handbook of Numerical Heat Transfer*, John Wiley & Sons, New York, pp. 673–722, 1988.
13. Howell, J. R.: "Application of Monte Carlo to heat transfer problems," in *Advances in Heat Transfer*, eds. J. P. Hartnett and T. F. Irvine, vol. 5, Academic Press, New York, 1968.
14. Walters, D. V., and R. O. Buckius: "Monte Carlo methods for radiative heat transfer in scattering media," in *Annual Review of Heat Transfer*, vol. 5, Hemisphere, New York, pp. 131–176, 1992.
15. Howell, J. R.: "The Monte Carlo method in radiative heat transfer," *ASME Journal of Heat Transfer*, vol. 120, no. 3, pp. 547–560, 1998.
16. Taussky, O., and J. Todd: "Generating and testing of pseudo-random numbers," in *Symposium on Monte Carlo Methods*, John Wiley & Sons, New York, pp. 15–28, 1956.
17. Modest, M. F., and S. C. Poon: "Determination of three-dimensional radiative exchange factors for the space shuttle by Monte Carlo," ASME paper no. 77-HT-49, 1977.
18. Barford, N. C.: *Experimental Measurements: Precision, Error and Truth*, Addison-Wesley, London, 1967.
19. Fröberg, C. E.: *Introduction to Numerical Analysis*, Addison-Wesley, Reading, MA, 1969.
20. Abramowitz, M., and I. A. Stegun (eds.): *Handbook of Mathematical Functions*, Dover Publications, New York, 1965.
21. Maltby, J. D.: "Three-dimensional simulation of radiative heat transfer by the Monte Carlo method," M.S. thesis, Colorado State University, Fort Collins, CO, 1987.
22. Burns, P. J., and J. D. Maltby: "Large-scale surface to surface transport for photons and electrons via Monte Carlo," *Computing Systems in Engineering*, vol. 1, no. 1, pp. 75–99, 1990.
23. Maltby, J. D., and P. J. Burns: "Performance, accuracy and convergence in a three-dimensional Monte Carlo radiative heat transfer simulation," *Numerical Heat Transfer – Part B: Fundamentals*, vol. 16, pp. 191–209, 1991.
24. Zeeb, C. N., P. J. Burns, K. Branner, and J. S. Dolaghan: "User's manual for Mont3d – Version 2.4," Colorado State University, Fort Collins, CO, 1999.
25. Larsen, M. E., and J. R. Howell: "Least-squares smoothing of direct-exchange areas in zonal analysis," *ASME Journal of Heat Transfer*, vol. 108, no. 1, pp. 239–242, 1986.
26. van Leersum, J.: "A method for determining a consistent set of radiation view factors from a set generated by a nonexact method," *International Journal of Heat and Fluid Flow*, vol. 10, no. 1, p. 83, 1989.
27. Lawson, D. A.: "An improved method for smoothing approximate exchange areas," *International Journal of Heat and Mass Transfer*, vol. 38, no. 16, pp. 3109–3110, 1995.
28. Loehrke, R. I., J. S. Dolaghan, and P. J. Burns: "Smoothing Monte Carlo exchange factors," *ASME Journal of Heat Transfer*, vol. 117, no. 2, pp. 524–526, 1995.
29. Daun, K. J., D. P. Morton, and J. R. Howell: "Smoothing Monte Carlo exchange factors through constrained maximum likelihood estimation," *ASME Journal of Heat Transfer*, vol. 127, no. 10, pp. 1124–1128, 2005.
30. Toor, J. S., and R. Viskanta: "A numerical experiment of radiant heat exchange by the Monte Carlo method," *International Journal of Heat and Mass Transfer*, vol. 11, no. 5, pp. 883–887, 1968.
31. Weiner, M. M., J. W. Tindall, and L. M. Candell: "Radiative interchange factors by Monte Carlo," ASME paper no. 65-WA/HT-51, 1965.
32. Modest, M. F.: "Determination of radiative exchange factors for three dimensional geometries with nonideal surface properties," *Numerical Heat Transfer*, vol. 1, pp. 403–416, 1978.
33. Heinisch, R. P., E. M. Sparrow, and N. Shamsundar: "Radiant emission from baffled conical cavities," *Journal of the Optical Society of America*, vol. 63, no. 2, pp. 152–158, 1973.
34. Shamsundar, N., E. M. Sparrow, and R. P. Heinisch: "Monte Carlo solutions — effect of energy partitioning and number of rays," *International Journal of Heat and Mass Transfer*, vol. 16, pp. 690–694, 1973.

Problems

Because of the nature of the Monte Carlo technique, most of the following problems require the development of a small computer code. However, all problem solutions can be outlined by giving relevant relations, equations, and a detailed flow chart.

8.1 Prepare a little Monte Carlo code that integrates $I(z) = \int_a^b f(z,x)\,dx$. Apply your code to a few simple integrals, plus

$$\mathrm{si}(z) = -\int_0^{\pi/2} e^{-z\cos x}\cos(z\sin x)\,dx = \mathrm{Si}(z) - \frac{\pi}{2}.$$

Note: Si(1) = 0.94608.

8.2 In a Monte Carlo simulation involving the plate of Problem 3.9 but of finite width w, a photon bundle is to be emitted from the plate with a wavelength of $\lambda = 2\,\mu$m. Find the emission point and direction of this photon bundle in terms of random numbers.

8.3 A triangular, isothermal surface as shown has the following spectral emittance:

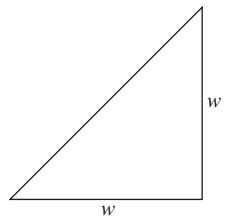

$$\epsilon_\lambda = \begin{cases} 0.1, & \lambda < 2\mu\text{m};\ \theta \le 60^\circ \\ 0.6, & \lambda > 2\mu\text{m};\ \theta \le 60^\circ \\ 0.0, & \text{all } \lambda;\ \theta > 60^\circ \end{cases}$$

For a Monte Carlo simulation

(a) find a point of bundle emission in terms of random numbers,

(b) find a wavelength of bundle emission in terms of random numbers,

(c) find a direction of bundle emission in terms of random numbers.

8.4 A semicircular disk as shown has a temperature distribution given by $T(r) = T_0/\left(1 + (r/R)^2\right)$, and its emittance is gray and nondiffuse with

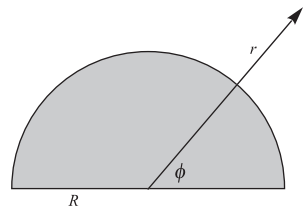

$$\epsilon' = \epsilon'_\lambda(\lambda, \theta, \psi) = \begin{cases} 0.6, & 0 \le \theta \le 30^\circ, \\ 0, & \theta > 30^\circ. \end{cases}$$

For a Monte Carlo simulation

(a) find a point of emission in terms of random numbers,

(b) find a direction of emission in terms of random numbers. You may leave your answer in simple implicit form.

8.5 A light pipe with direct solar irradiation is to be investigated via a Monte Carlo method. Such a device consists of a straight or curved tube covered with a highly-reflective material to pipe light into a room. At visible wavelengths the reflectance from the pipe wall is $\rho'_\lambda(\theta_{out}) = 1.5\rho_\lambda \cos\theta_{out}$, with reflection angle θ_{out} measured from the local surface normal, and visible light intensity due to direct sunshine may be approximated by

$$L_\lambda = K_\lambda I_{\lambda,\text{sun}} = C \exp[-A^2(\lambda - \lambda_0)^2],\ \lambda_0 = 0.56\mu\text{m},\ A = 20/\mu\text{m}.$$

(a) Find the pertinent relationship to determine wavelengths of emission as a function of random number.

(b) Find an expression for reflection angle vs. random number.

8.6 At the Aaronsburg (Pennsylvania) Apple Fest you have won a large piece of elderberry pie (yumh!) as shown. The wheels in the oven must have been spinning, because it appears that the number of elderberries per unit area increases linearly proportional with radius! If there are 1000 elderberries otherwise randomly distributed on the slice, make a scatter plot of elderberries on the pie slice.

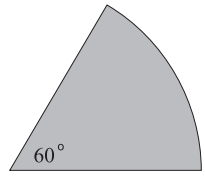

8.7 Consider a black disk $0 \le r \le R$ with temperature distribution $T^4(r) = T_0^4 e^{-C(r/R)^2}$. Develop the random number relations for points of emission; draw random numbers for 1000 emission points and draw them in a scattergram for the cases of $C = 0$ and $C = 5$. Use $R = 10$ cm.

8.8 A disk of radius R is opposed by a square plate (sides of length R) parallel to it, and a distance R away. Find the view factor from disk to square plate. Use 100,000 bundles, plotting updated results after every 5,000 bundles.

8.9 Consider two infinitely long parallel plates of width w spaced a distance h apart. (see Configuration 32 in Appendix D).

(a) Calculate F_{1-2} via Monte Carlo for the case that the top plate is horizontally displaced by a distance L. Use $L = h = w$.

(b) Calculate F^s_{1-2} via Monte Carlo for the case that both plates are specular (with identical reflectances $\rho^s_1 = \rho^s_2 = 0.5$), but not horizontally displaced. Use $L = 0, h = w$.

Prepare a figure similar to Fig. 8-2, also including analytical results for comparison.

8.10 Two directly opposed quadratic plates of width $w = 10\,\text{cm}$ are spaced a distance $L = 10\,\text{cm}$ apart, with a third centered quadratic plate of dimension $b \times b$ ($b = 5\,\text{cm}$) in between at a distance $l = 5\,\text{cm}$ from the bottom. Determine the view factor F_{1-2} via Monte Carlo. In order to verify your code (and to have a more flexible tool) it may be best to allow for arbitrary and different top and bottom w as well as b.

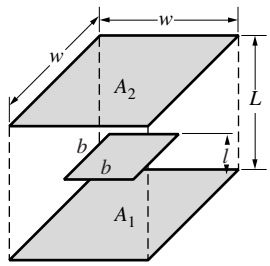

8.11 Consider two concentric parallel disks of radius R, spaced a distance H apart. Both plates are isothermal (at T_1 and T_2, respectively), are gray diffuse emitters with emittance ϵ, and are gray reflectors with diffuse reflectance component ρ^d and purely specular component ρ^s. Write a computer code that calculates the generalized exchange factor $\mathscr{F}_{1\to2}$ and, taking advantage of the fact that $\mathscr{F}_{1\to2} = \mathscr{F}_{2\to1}$, calculate the total heat loss from each plate. Compare with the analytical solution treating each surface as a single node.

8.12 Repeat Problem 8.11, but calculate heat fluxes directly, i.e., without first calculating exchange factors.

8.13 Determine the view factor for Configuration 39 of Appendix D, for $h = w = l$. Compare with exact results.

8.14 Consider the conical geometry of Problem 5.9: breaking up the sidewall into strips (say 4), calculate all relevant view factors (base-to-rings, ring-to-rings) via Monte Carlo.

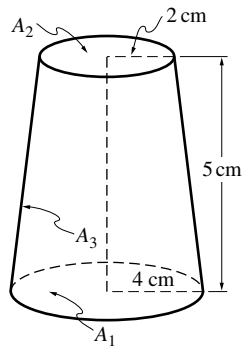

8.15 Reconsider Problem 5.30: *(a)* find the solution by writing a small Monte Carlo program, and *(b)* augment this program to allow for nongray, temperature-dependent emittances.

8.16 Repeat Problem 5.33 for $T_1 = T_2 = 1000\,\text{K}$, $\epsilon_1 = \epsilon_2 = 0.5$. Use the Monte Carlo method, employing the energy partitioning of Sparrow and coworkers [33, 34].

8.17 Repeat Problem 5.34. Compare with the exact solutions for several values of ϵ.

8.18 Repeat Problem 6.3, using the Monte Carlo method. Compare with the solution from Chapter 6 for a few values of D/L and ϵ, and $T_1 = 1000\,\text{K}$, $T_2 = 2000\,\text{K}$. How can the problem be done by emitting bundles from only one surface?

8.19 Repeat Problem 6.10 using the Monte Carlo method.

8.20 Repeat Problem 6.23 using the Monte Carlo method.

8.21 Repeat Example 7.3 using the Monte Carlo method.

8.22 Repeat Example 7.4 using the Monte Carlo method.

8.23 Repeat Problem 7.20 using the Monte Carlo method.